Hindawi
Shock and Vibration
Volume 2024, Article ID 3495503, 11 pages
https://doi.org/10.1155/2024/3495503

Research Article

Dynamic Performance Analysis of Semiactive Vehicle ISD Suspension Based on the Power-Driven-Damper Strategy

Yujie Shen,[1] **Jinsen Wang**,[1] **Fu Du**,[2,3] **Xiaofeng Yang**,[4] **Yanling Liu**,[4] **and Long Chen**[1]

[1]*Automotive Engineering Research Institute, Jiangsu University, Zhenjiang 212013, China*
[2]*School of Mechanical Engineering, Beijing Institute of Technology, Beijing 100081, China*
[3]*Chinese Scholar Tree Ridge Laboratory, China North Vehicle Research Institute, Beijing 100072, China*
[4]*School of Automotive and Traffic Engineering, Jiangsu University, Zhenjiang 212013, China*

Correspondence should be addressed to Yujie Shen; shenyujie@ujs.edu.cn

Received 22 August 2023; Revised 29 February 2024; Accepted 2 March 2024; Published 13 March 2024

Academic Editor: Piotr Folęga

Copyright © 2024 Yujie Shen et al. This is an open access article distributed under the Creative Commons Attribution License, which permits unrestricted use, distribution, and reproduction in any medium, provided the original work is properly cited.

In this paper, the vehicle ISD (inerter-spring-damper) suspension and power-driven-damper control strategy are combined to the suspension design, and the power-driven-damper semiactive ISD suspension is proposed. The dynamic models of the passive suspension S1 and two semiactive ISD suspensions S2 and S3 are established. Based on the port-controlled Hamiltonian theory, the power-driven-damper semiactive control strategy is designed by analyzing the power transfer of suspension S3. Then, the parameters of the two models are optimized by the particle swarm optimization algorithm, and the optimization results show that the suspension S3 has better performance. The influence of the semiactive damping coefficient, the spring stiffness, and the inertance on the vibration suppression performance is investigated based on the suspension S3. The effect of parameter perturbation on power-driven-damper semiactive vehicle ISD suspension illustrates that the designed semiactive vehicle ISD suspension has better ride comfort in a wider range frequency and good robust performance.

1. Introduction

Vehicle suspension is an essential component of the chassis system, and it can buffer the impact of road roughness [1, 2] and play a decisive role in providing passengers with excellent ride comfort performance [3, 4]. Therefore, improving the performance of suspension has important engineering significance. As we all know, the traditional passive suspension consisting of springs and dampers has been widely used for its low price and practicality [5]. However, with the rapid development of automotive technology, the traditional passive suspension is brutal to meet people's demand for better comfort. The performance enhancement of passive suspension has reached a bottleneck, and this situation is not improved until Smith [6] invented the inerter element, a passive mechanical structure that can generate a force proportional to the relative acceleration of its two ends. With the introduction of inerter into the field of vehicle vibration isolation, the inherent form of traditional suspension "spring-damping" is broken, and a new "inerter-spring-damper" suspension (called ISD suspension) appears. The vehicle ISD suspension has been widely studied by scholars, and it is proven to have good vibration suppression performance [7, 8].

The research illustrates that compared with the vibration suppression performance of traditional suspension, the performance of vehicle ISD suspension of many layouts is much better [9, 10]. Under different road excitations, the dynamic characteristics of suspension are studied, and the results illustrate that the vibration suppression performance of vehicle ISD suspension is very superior [11]. Two types of vehicle ISD suspension layouts are designed and analyzed in the frequency domain, and it is shown that the vibration in the offset frequency bands of the body resonance can be suppressed by vehicle ISD suspension [12]. Moreover, the performance of heavy vehicles with inerter is greatly improved; the research indicates that the vertical vibration of

heavy vehicle can be effectively reduced by the vehicle ISD suspension, and it is more prominent in the low frequency band [13, 14].

Because the parameters of the passive suspension is not adjustable and the suspension can only obtain the best vibration suppression performance under a specific road input, the control strategy [15, 16] is introduced into the suspension system, and the suspension which can actively adjust the parameters is studied. Active suspension is to control the actuator output for power so that the body attitude can reach an ideal state under different road conditions. Compared with passive suspension, the ride comfort and handling stability of active suspension have been effectively improved [17–19], but the high manufacturing cost restricts its further wide application. In contrast to active control, semiactive control [20] necessitates a lower amount of external energy for the generation of control force and also diminishes structural complexity. This control approach has found application in areas such as earthquake resistance and suspension systems [21, 22]. The concept of semiactive suspension is proposed by Karnopp [23], which can adjust the spring stiffness and damping coefficient according to the road input to improve ride comfort. Research indicates that compared with passive suspension, semiactive suspension has better performance [24]. Under the idea of semiactive suspension, a series of excellent semiactive control strategies come up and are applied to suspension systems in order to further improve the vibration suppression performance of suspension, including classic two-state skyhook (SH) [25], acceleration-driven-damper (ADD) [26], power-driven-damper (PDD) [27], mixed skyhook-acceleration driven damper (SH-ADD) [28], and mixed skyhook and power-driven-damper (SH-PDD) [29]. The research shows that the ADD control strategy can suppress the vibration of the body in the high frequency band effectively, but the ADD control strategy is a control strategy that switches according to the value of acceleration, and obvious shake exists when the body acceleration is zero, while the PDD control strategy can suppress the vibration of the body effectively without producing obvious shake. The vehicle ISD suspension has better vibration suppression effect in the low frequency band, but it does not have good performance in the high frequency band. By combining the vehicle ISD suspension with the power-driven-damper control strategy, vibration suppression can be achieved over a wider range frequency, thus improving ride comfort. This paper is devoted to the study of vibration suppression mechanism of power-driven- damper vehicle ISD suspension. The effects of the damping coefficient, variable spring stiffness, and variable inertance on vibration suppression are also studied to draw some conclusions. The arrangement of this paper is as follows.

In Section 2, three suspension models are built, the explicit expression of the power-driven-damper control strategy is derived based on the port-controlled Hamiltonian theory, and the optimal parameters of suspension are obtained by particle swarm optimization (PSO) which has fast convergence speed and is easy to obtain the global optimal solution [30]. Effect of the damping coefficient on vibration suppression performance is analyzed in Section 3. In Section 4, the influence of variable spring stiffness and variable inertance on the semiactive vehicle ISD suspension is also studied. Finally, some conclusions are drawn in Section 5.

2. Dynamic Model of Vehicle ISD Suspension Based on the Power-Driven-Damper

2.1. Dynamic Model of Vehicle ISD Suspension. Quarter suspension is a two-degree-of-freedom model obtained by simplifying the vehicle suspension system according to its structure and type, and it is the most commonly used basic model to study the control law and vibration suppression mechanism of vehicle suspension, as shown in Figure 1. In this paper, three simple suspension layouts are established, which are traditional passive suspension S1, power-driven-damper vehicle ISD suspension S2, and power-driven-damper vehicle ISD suspension S3, as shown in Figure 2 [31].

In Figures 1 and 2, m_s is the sprung mass, m_u is the unsprung mass, z_s is the vertical displacements of the sprung mass, z_u is the vertical displacements of the unsprung mass, z_r is the random road input, K_t is the equivalent spring of the tire, and M represents the structure of the suspension, including the three structures shown in Figure 2. For suspension S1, the damper and the spring are arranged in parallel. For suspension S2, the semiactive damper and the inerter are arranged in parallel. For suspension S3, the semiactive damper and the intermediate structure $T(s)$ are also arranged in parallel, where $T(s)$ is an intermediate structure comprising an inerter and a spring connected in series. K is the support spring, b is the inerter, c is the damper, c_p is the semiactive damper, and k is the auxiliary spring. The dynamic motion equations of the suspensions are as follows:

$$\begin{cases} m_s\ddot{z}_s + K(z_s - z_u) + c(\dot{z}_s - \dot{z}_u) = 0, \\ m_u\ddot{z}_u + K_t(z_u - z_r) - K(z_s - z_u) - c(\dot{z}_s - \dot{z}_u) = 0, \end{cases}$$
$$\begin{cases} m_s\ddot{z}_s + K(z_s - z_u) + c_p(\dot{z}_s - \dot{z}_u) + b(\dot{z}_s - \dot{z}_u) = 0, \\ m_u\ddot{z}_u + K_t(z_u - z_r) - K(z_s - z_u) - c_p(\dot{z}_s - \dot{z}_u) - b(\dot{z}_s - \dot{z}_u) = 0, \end{cases} \tag{1}$$
$$\begin{cases} m_s\ddot{z}_s + K(z_s - z_u) + c_p(\dot{z}_s - \dot{z}_u) + T(s)(\dot{z}_s - \dot{z}_u) = 0, \\ m_u\ddot{z}_u + K_t(z_u - z_r) - K(z_s - z_u) - c_p(\dot{z}_s - \dot{z}_u) - T(s)(\dot{z}_s - \dot{z}_u) = 0. \end{cases}$$

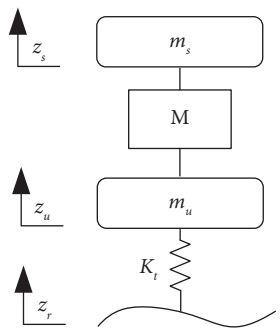

Figure 1: The quarter-car model.

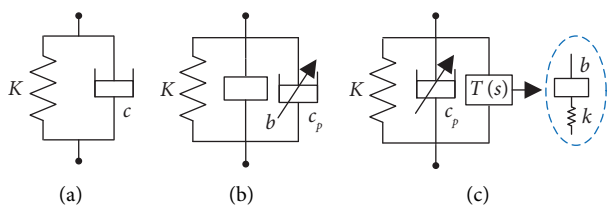

Figure 2: The suspension layouts. (a) S1 (b) S2 (c) S3.

2.2. Port-Controlled Hamilton System and the Power-Driven-Damper Control Strategy. In suspensions S1 and S2, the controllable damper is the only energy dissipating element, and the others are the energy storage element, which is a typical port-controlled Hamiltonian system [27], and can be expressed as follows:

$$\begin{aligned} \dot{x} &= \left[J_1(x,v) - R_1(x,v)\right]\frac{\partial H}{\partial x}(x) + g(x,v)u \\ y &= g^T(x,v)\frac{\partial H}{\partial x}(x) - \left[J_2(x,v) - R_2(x,v)\right]u \\ J_i(x,v) &= -J_i^T(x,v) \qquad i = 1,\ 2, \\ R_i(x,v) &= -R_i^T(x,v) \qquad i = 1,\ 2, \end{aligned} \tag{2}$$

where u is the pavement input disturbance variable, v is the input variable of controllable damping, y is the output variable, x is the state variable, $J_i(x,v)$ is the interconnection matrix of the system, $R_i(x,v)$ is the damping dissipation matrix, $H(x)$ is the Hamiltonian energy function of the system, and $g(x, v)$ is the function related to the state variable. The power balance equation of the port-controlled Hamiltonian system can be expressed as follows:

$$\frac{dH}{dt} = y^T u - \frac{\partial H^T}{\partial x}R_1(x,v)\frac{\partial H}{\partial x} - u^T R_2(x,v)u = y^T u - d(v,x). \tag{3}$$

The power dissipation equation of the system can be expressed as follows:

$$d(v,x) = \frac{\partial H^T}{\partial x}R_1(x,v)\frac{\partial H}{\partial x} + u^T R_2(x,v)u. \tag{4}$$

In order to maximize the passenger riding comfort, the power-driven-damper control strategy gives priority to reducing body acceleration. The control strategy can be expressed as follows:

$$v: \begin{cases} \arg\max(\dot{H} + d), & \text{if } \arg\max(\dot{H} + d) < W_d, \\ \arg\min(\dot{H} + d), & \text{if } \arg\max(\dot{H} + d) \geq W_d, \\ W_d = \dot{H} + d(v,x), & \text{otherwise}, \end{cases} \tag{5}$$

where W_d denotes the desired level of power, which equals zero, and $d(v, x)$ denotes all the energy dissipations. Taking the suspension S3 as an example, the storage power can be expressed as follows:

$$\dot{H} = K(z_s - z_u)(\dot{z}_s - \dot{z}_u) + T(s)(\dot{z}_s - \dot{z}_u)^2. \tag{6}$$

The dissipated power can be expressed as follows:

$$d(c_p, x) = c_p(\dot{z}_s - \dot{z}_u)^2. \tag{7}$$

The total suspension power can be expressed as follows:

$$W_d = \dot{H} + d(c_p, x) = K(z_s - z_u)(\dot{z}_s - \dot{z}_u) + c_p(\dot{z}_s - \dot{z}_u)^2 + T(s)(\dot{z}_s - \dot{z}_u)^2. \tag{8}$$

The control strategy set in this paper is as follows: when the net input power in suspension is less than zero, c_p is the maximum value. When the net input power in suspension is greater than or equal to zero, c_p takes the minimum value; When the net input power of suspension is zero but the relative displacement of suspension is not zero, that is, when the relative speed is zero and the relative displacement of suspension is not zero, c_p is taken as the average value of the maximum and minimum values; this process is regarded as the transition stage. In the last mode, the c_p value ensures zero net input power. The power-driven-damper control strategy avoids the switching conditions associated with body acceleration and, therefore, can suppress shake to a large extent. The conditions to be met for the controllable damping coefficient c_p are as follows [32]:

$$c_p = \begin{cases} c_{\max}, K(z_s - z_u)(\dot{z}_s - \dot{z}_u) + c_{\max}(\dot{z}_s - \dot{z}_u)^2 + T(s)(\dot{z}_s - \dot{z}_u)^2 < 0, \\ c_{\min}, K(z_s - z_u)(\dot{z}_s - \dot{z}_u) + c_{\min}(\dot{z}_s - \dot{z}_u)^2 + T(s)(\dot{z}_s - \dot{z}_u)^2 \geq 0, \\ \dfrac{c_{\max} + c_{\min}}{2}, (\dot{z}_s - \dot{z}_u) = 0 \,\&\, (z_s - z_u) \neq 0, \\ \dfrac{-K(z_s - z_u) - T(s)(\dot{z}_s - \dot{z}_u)}{(\dot{z}_s - \dot{z}_u)}, \quad \text{otherwise.} \end{cases} \tag{9}$$

2.3. Optimization of Suspension Structure Parameters. To obtain the best performance of suspension, it is necessary to optimize the parameters of suspension. In this paper, the particle swarm optimization (PSO) with fast convergence speed and easy to find the global optimal solution is selected.

The basic idea of particle swarm optimization is to design a massless particle to simulate birds, set it in a certain space range, and each particle searches for the optimal solution p_{best} in the space separately, and shares the individual optimal solution with other particles in the population. Finally, the best solution among all the individual optimal solutions is regarded as the global optimal solution g_{best} [33]. The updated formulas for particle velocity and position properties are as follows:

$$\begin{aligned} V^{m+1} &= \omega V^m + c_1 r_1 (P^m_{\text{best}} - X^m) + c_2 r_2 (g^m_{\text{best}} - X^m), \\ X^{m+1} &= X^m + V^{m+1}. \end{aligned} \tag{10}$$

In the formula, ω represents the inertia weight, the general value is [0.8, 1.2]; c_1 and c_2 represent learning factors or acceleration constants; r_1 and r_2 represent random numbers in [0, 1]; m represents the number of iterations; p_{best} represents the individual extreme value; g_{best} represents the group extreme value; V^m represents the velocity of the particle when the number of iterations is m; V^{m+1} represents the velocity of the particle when the number of iterations is $m+1$; X^m represents the position of the particle when the number of iterations is m; and X^{m+1} represents the position of the particle when the number of iterations is $m+1$. The flowchart of the optimization process is shown in Figure 3.

In this paper, the main spring stiffness K, auxiliary spring stiffness k, inertance b, maximum adjustable damping coefficient $c_{\max}$, and minimum adjustable damping coefficient $c_{\min}$ are taken as the individual to be sought, the parameters are optimized with comfort as the guidance and the RMS (root mean square) of body acceleration as the optimization objective. Since the vehicle vibration response basically conforms to the normal distribution, according to the normal distribution probability integral principle, if RMS of the dynamic tire load is less than one third of the static load G, equaling m_s plus m_u, the odds that the wheel jumps off the road profile is less than 0.15%. If the RMS of the suspension working space is under one third of its threshold value $[f_d]$, the suspension working space can maintain a safe range within 99.7% functioning time [34]. Generally, the value of $[f_d]$ is 7–9 cm, and 8 cm is selected in this paper. Therefore, the RMS of the dynamic tire load and the RMS value of the suspension working space are selected as constraints, and they are less than 1217 N and 0.027 m, respectively. The boundaries of optimized design variables are as follows: main spring is the primary support spring, responsible for providing support, and its value needs to consider practical applications. Therefore, the value range of K is between $10000\,\text{N}\cdot\text{m}^{-1}$ and $25000\,\text{N}\cdot\text{m}^{-1}$. Auxiliary spring stiffness does not need to be excessively large. Therefore, the value of k ranges from $0\,\text{N}\cdot\text{m}^{-1}$ to $10000\,\text{N}\cdot\text{m}^{-1}$. The selection of the damping coefficient and inertance is appropriate for practical applications. The range of damping coefficient is from $0\,\text{N}\cdot\text{s}\cdot\text{m}^{-1}$ to $10000\,\text{N}\cdot\text{s}\cdot\text{m}^{-1}$, and the range of inertance is from 0 kg to 1000 kg.

In this paper, the pavement input model is a random pavement input model and the expression is as follows:

$$\dot{z}_r(t) = -0.111\left[u z_r(t) + 40\sqrt{G_q(n_0)u}\,w(t)\right]. \tag{11}$$

In the formula, u is the vehicle speed, $z_r(t)$ is the vertical input displacement, $w(t)$ is the white noise with an average value of 0, and $G_q(n_0)$ is the road roughness coefficient. In this paper, the set speed is 100 km/h, grade C pavement is selected, and the road roughness coefficient is $256 \times 10^{-6}\,\text{m}^3$.

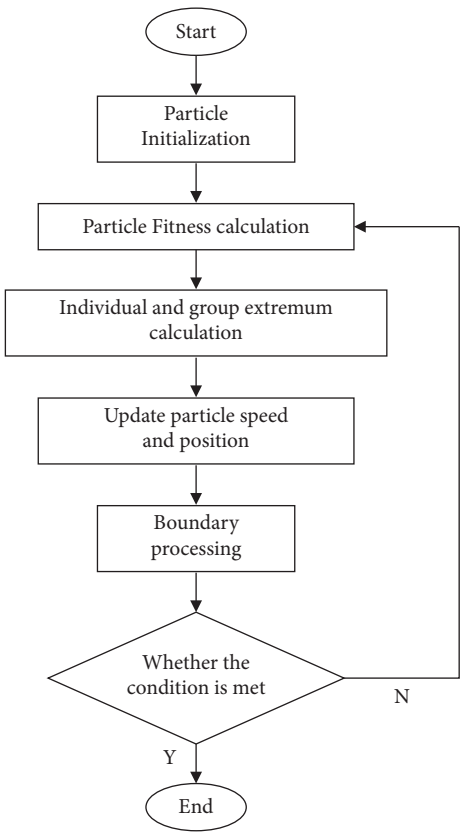

Figure 3: Parameter optimization flowchart.

The parameters of the quarter-car model are shown in Table 1 [35], and the optimized results are shown in Table 2.

Based on the parameter optimization, the three suspensions are simulated, respectively, and the comparison of their values are shown in the Table 3.

In this paper, the suspension is comfort oriented and the most important evaluation index is body acceleration; the responses are shown in Figure 4.

From Table 3 and Figure 4, it can be seen that the vibration suppression performances of the semiactive vehicle ISD suspensions based on the power-driven-damper are significantly improved. From the frequency domain diagram, it can be seen that compared with suspension S1, the gains of body acceleration of suspension S2 and suspension S3 are smaller in the whole frequency domain; this result indicates that that the semiactive ISD suspension based on power-driven-damper effectively achieves vibration suppression in the wider range frequency. From the time domain results, it can be seen that compared with suspension S1, the RMS of the body acceleration of suspension S2 is reduced by 25.3% and the RMS of body acceleration of suspension S3 is reduced by 29.8%. Compared with suspension S2, the RMS values of body acceleration of S3 is better in the whole time domain simulation process. It can be seen that the performance of suspension S3 is obviously superior to suspension S2 in terms of the frequency analysis and time domain analysis.

Table 1: Model parameters.

Parameters	Values
Sprung mass (m_s/kg)	320
Unsprung mass (m_u/kg)	45
Damping coefficient (c/N·s·m^{-1})	1500
Stiffness of spring (K/N·m^{-1})	22000
Stiffness of tire (K_t/N·m^{-1})	190000

Table 2: Optimized parameters.

Suspension class	Parameters	Values
Suspension S2	Stiffness of support spring (K/N·m^{-1})	15530
	Inertance (b/kg)	3.8
	Maximum damping coefficient (c_{max}/N·s·m^{-1})	9885
	Minimum damping coefficient (c_{min}/N·s·m^{-1})	891
Suspension S3	Stiffness of support spring (K/N·m^{-1})	10023
	Inertance (b/kg)	1000
	Stiffness of auxiliary spring (k/N·m^{-1})	2040
	Maximum damping coefficient (c_{max}/N·s·m^{-1})	9995
	Minimum damping coefficient (c_{min}/N·s·m^{-1})	824

3. Impact of the Power-Driven-Damper Coefficient on Vehicle ISD Suspension Performance

The core of the power-driven-damper control strategy is to change the damping coefficient according to the road input so as to improve the vibration suppression performance of the suspension. In order to further study the mechanism of the power-driven-damper control strategy in vehicle ISD suspension based on suspension S3, the body acceleration, the suspension working space, and the dynamic tire load are deemed as response variables while the c_{max} and c_{min} are deemed as independent variables, and the influence of damping coefficient on vibration suppression performance is analyzed. The responses are shown in Figures 5–7, and the asterisk in the figure is marked as the optimal value point of optimization.

Figure 5 shows the change of body acceleration with the variation of c_{max} and c_{min}. It can be seen that when the value of c_{max} increases gradually in the range of 0–10000 N·s·m^{-1}, the RMS of body acceleration decreases rapidly at first and then decreases slowly after a turning point is reached. With an increase of the value of c_{min}, the RMS of body acceleration first decreases and then increases, and when the value of c_{max} is small, the rate of change is large.

Figure 6 shows the change of the suspension working space with the variation of c_{max} and c_{min}; it can be seen that with an increase of value of c_{max}, the RMS of suspension working space decreases rapidly at first and increases slowly after an inflection point is reached. With an increase of the value of c_{min}, the RMS of suspension working space

Table 3: RMS values comparison of suspension.

RMS values	Suspension S1	Suspension S2	Suspension S3
Vehicle body acceleration (m/s^2)	1.7120	1.2798	1.2033
Suspension working space (m)	0.037	0.0153	0.0150
Dynamic tire load (N)	971.0	1216.9	1216.9

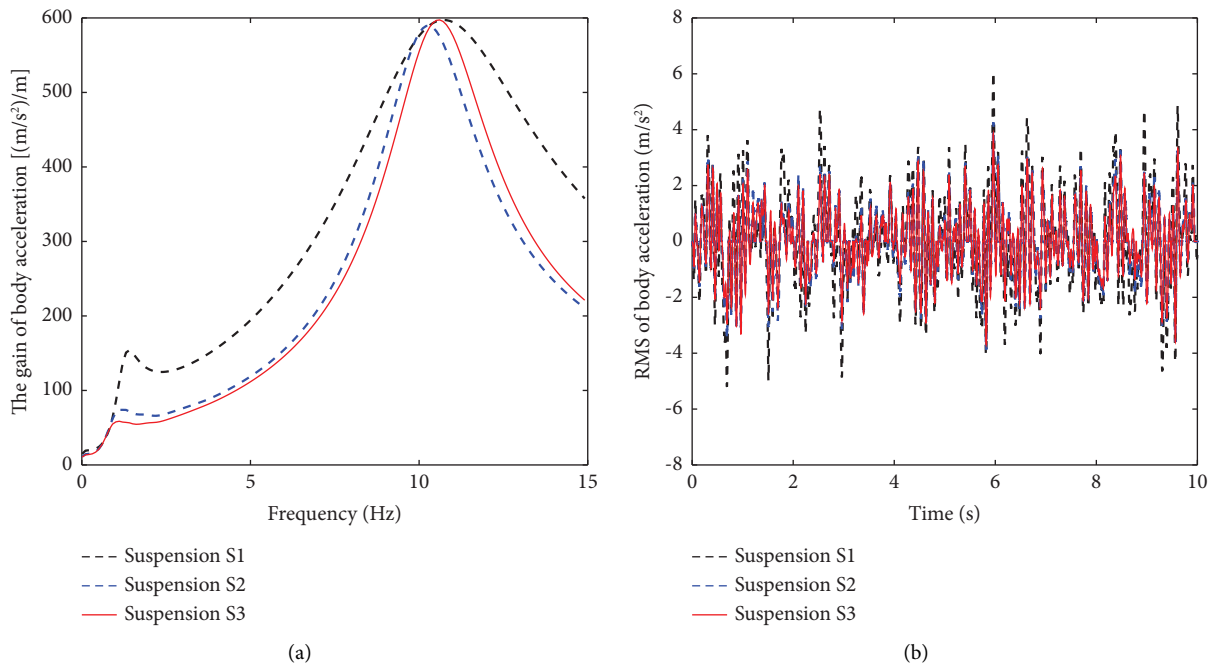

Figure 4: Responses of vehicle body acceleration.

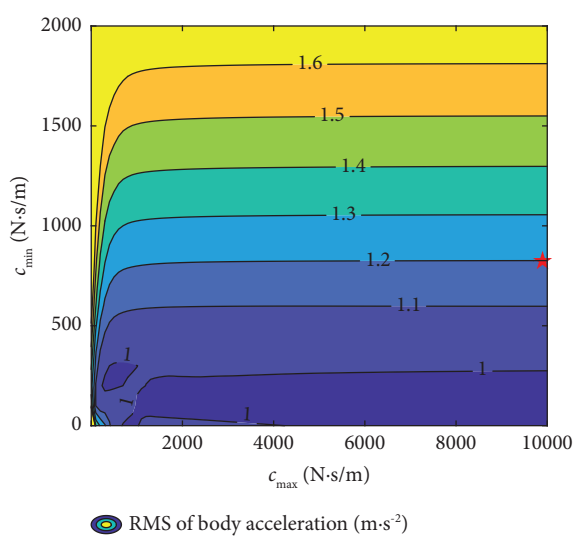

Figure 5: The change of body acceleration with the variation of c_{max} and c_{min}.

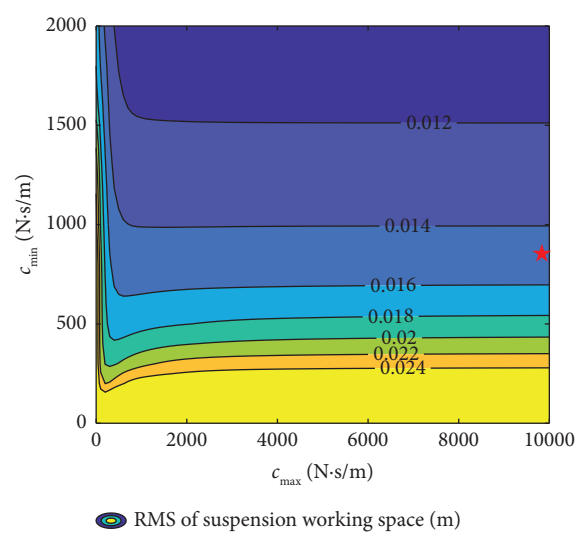

Figure 6: The change of suspension working space with the variation of c_{max} and c_{min}.

decreases gradually, and the decreasing speed decreases with an increase of value of c_{min}.

Figure 7 shows the change of the dynamic tire load with the variation of c_{max} and c_{min}; it can be seen that with an increase of the value of the c_{max}, the RMS of dynamic tire load decreases rapidly at first and then decreases slowly after an inflection point is reached. With an increase of the value of c_{min}, the RMS of dynamic tire load decreases gradually, and the decreasing speed decreases with an increase of value of c_{min}.

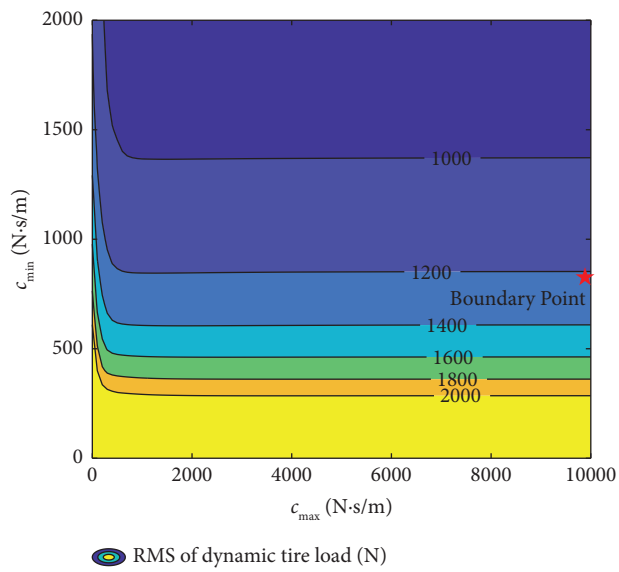

Figure 7: The change of dynamic tire load with the variation of c_{max} and c_{min}.

It can be concluded that the trend of body acceleration is different, but the trends of RMS of the suspension working space and RMS of the dynamic tire load are similar. When the value of c_{max} is large and the value of c_{min} is small, the RMS of body acceleration is small, but when the value of c_{max} and the value of c_{min} are large, the RMS of the dynamic tire load and RMS of the suspension working space are small. Since it is a comfort-oriented suspension system, the value of c_{max} should be as large as possible and the value of c_{min} should be as small as possible in order to obtain a small RMS of body acceleration within the constraints. In this paper, when the RMS of body acceleration reaches the minimum value, the RMS of the dynamic tire load reaches the boundary value of the constraint condition, and the RMS of the working space is still within the constraint range. The abovementioned studies show the effect of the damping coefficient variation on the vibration suppression performance and also verify the correctness of the parameter optimization.

4. Impact of the Parameters Perturbation on Vehicle Suspension Performance

In this section, the effect of the parameters perturbation on suspension performance will be analyzed in detail. According to the above research, the performance of the suspension S3 is the best, thus suspension S3 is selected as the research object. According to the parameter optimization results, the values of auxiliary springs are increased and decreased by 50%, while other parameters are unchanged, as shown in Table 4. Figure 8 shows the gains of body acceleration, suspension working space, and dynamic tire load with variable stiffness while the damping coefficient and the inertance are constant; the comparison of peak data is shown in Table 5.

Figure 8(a) shows the gains of body acceleration of variable stiffness. It can be seen that the peak values become larger with the increase of the stiffness both in the low frequency and high frequency band. Figure 8(b) shows the gains of the suspension working space of variable stiffness. The peak values in the low frequency band become larger with the increase of the stiffness, but the peak values in the high frequency band become smaller with the increase of the stiffness. Figure 8(c) shows the gains of the dynamic tire load of variable stiffness. With the increase of stiffness, the peak values in the low frequency band become larger, but with the increase of stiffness, the peak values in the high frequency band become smaller. It can be concluded that the variable stiffness results in different change trends of the three performance indices, but all of the peak value variations are less than 10% in Table 5, which indicates that the suspension of this structure has good robustness.

Table 4: Perturbation parameters.

Parameters	Reference value	−50%	+50%
Auxiliary spring (k/N·m^{-1})	2040	1020	3060

Figure 9 shows the changes of RMS of body acceleration, RMS of suspension working space, and RMS of dynamic tire load with the inertance varying from 0 kg to 1000 kg.

It can be seen that the RMS of body acceleration undergoes a rapid increase with the rise of the inertance, followed by a sharp decline. Subsequently, it undergoes a slight increase before gradually decreasing again. With the increase of the inertance, the RMS of suspension working space undergoes a brief period of slight decrease, followed by a rapid increase and then a swift decrease. Subsequently, it undergoes two stages of first increasing and then decreasing, and the magnitude of the change gradually decreases. Eventually, it slowly rises. With the increase of the inertance, the RMS of the dynamic tire load undergoes three stages of rapid decrease followed by rapid increase, with the magnitude of change gradually diminishing as the inertance increases. Following this stage, the RMS of the dynamic tire

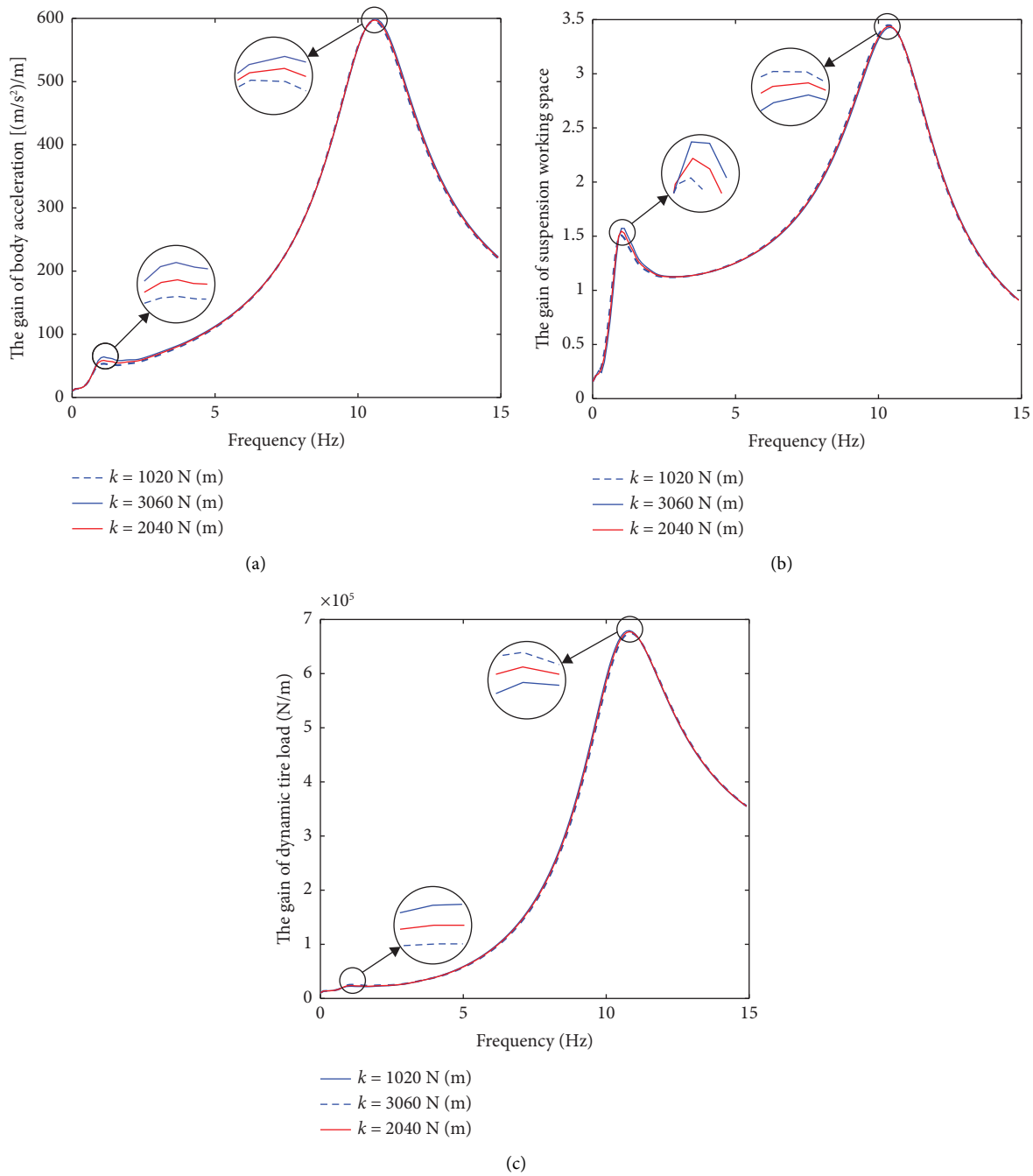

Figure 8: Gains of variable stiffness.

Table 5: Comparison of peak data.

Peak frequency	Evaluation index	$k = 2040$ N·m^{-1}	$k = 1020$ N·m^{-1}	Variation (%)	$k = 3060$ N·m^{-1}	Variation (%)
Low	Body acceleration (m/s^2)	58.6	53.4	−8.87	64.2	9.56
	Suspension working space	0.0154	0.0151	−1.94	0.0157	1.94
	Dynamic tire load (kN/m)	23.8	25.4	−6.72	22.4	5.88
High	Body acceleration (m/s^2)	597.3	595.5	−0.30	599.1	0.30
	Suspension working space	0.0344	0.0345	0.29	0.0343	−0.29
	Dynamic tire load (kN/m)	677.2	675.0	0.32	679.4	−0.32

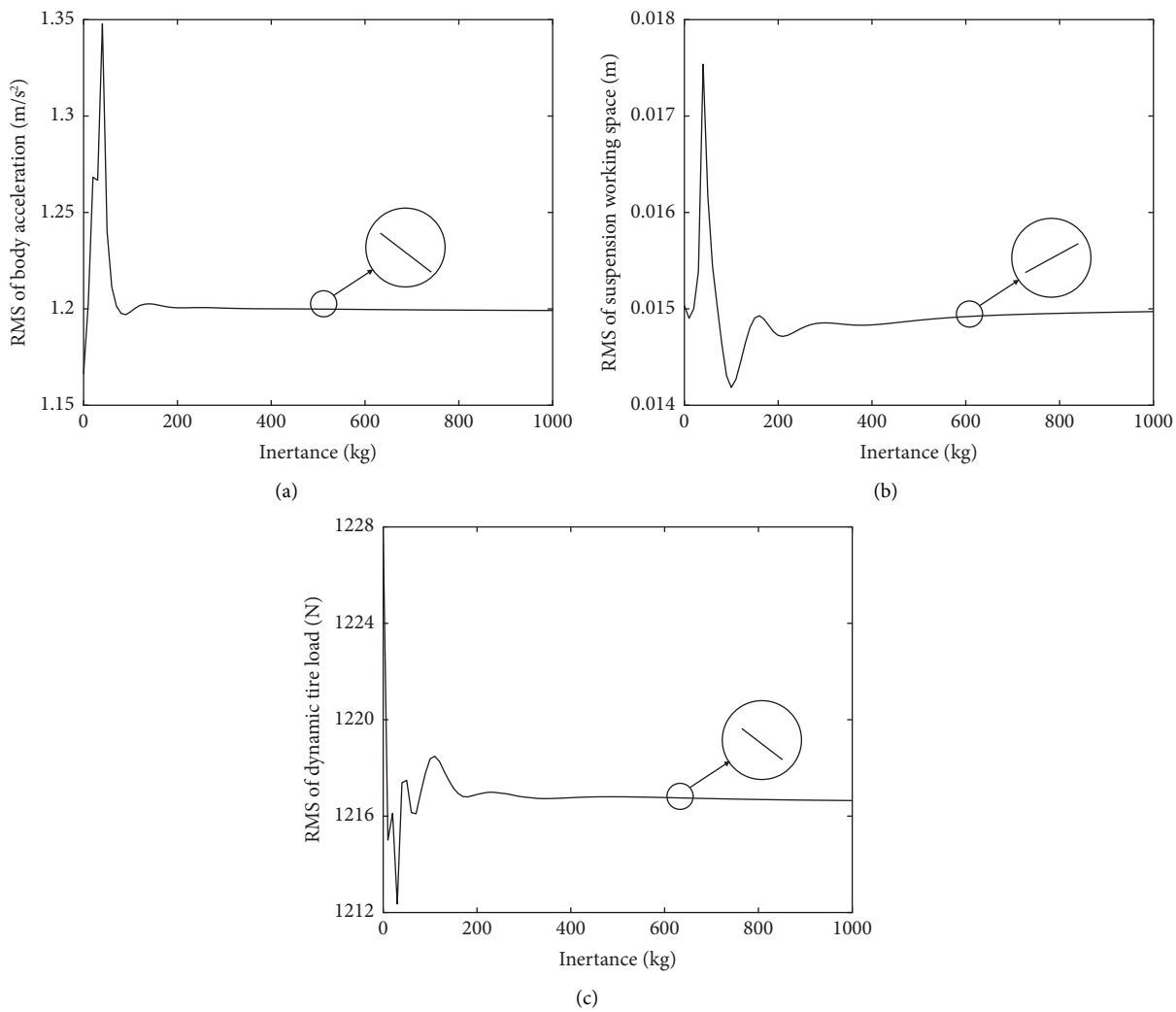

Figure 9: Changes of vibration suppression performance of variable inertance.

load decreases slowly. Since it is a comfort-oriented suspension, the body acceleration should be as small as possible within the constraint conditions, and it can be seen that when the inertance is 1000 kg, the body acceleration is the minimum value that satisfies the constraint conditions.

5. Conclusion

In this paper, the performance of the semiactive vehicle ISD suspension based on the power-driven-damper strategy is investigated. Three-type suspension dynamic models are established, and the expression of the power-driven-damper control strategy is obtained according to the port-controlled Hamiltonian theory. The particle swarm optimization is used to optimize the parameters of the suspension, and the optimal structure is suspension S3. The suspension S3 is selected as the research object, and the influence of the semiactive damping coefficient on suspension performance is analyzed. Results illustrate that the designed semiactive vehicle suspension has a better vibration isolation performance in the wider range frequency, and larger $c_{\max}$ value and smaller $c_{\min}$ value are more beneficial to obtain good ride comfort performance within the constraint range. Then, the impact of the spring stiffness perturbation and the inertance variation on suspension performance is also studied; the results illustrate that variable stiffness results in different variation trends of the body acceleration, suspension working space, and dynamic tire load, but all of the peak value changes are less than 10%. A big inertance value is also suggested for the comfort-oriented suspension design, but the actual application cost of the device should also be considered. The research results may provide certain engineering-guiding significance for the parameter design of the semiactive vehicle ISD suspension.

Data Availability

The data used to support the findings of the study are available from the corresponding author upon request.

Conflicts of Interest

The authors declare that they have no conflicts of interest.

Acknowledgments

This work was supported by National Natural Science Foundation (Grant no. 52072157), the Natural Science Foundation of Jiangsu Province (Grant no. BK20200911), the Postgraduate Research and Practice Innovation Program of Jiangsu Province (Grant no. SJCX22_1850), and Young Elite Scientists Sponsorship Program by CAST (Grant no. 2022QNRC001).

References

[1] Y. Li, X. F. Yang, Y. J. Shen, Y. L. Liu, and W. Wang, "Optimal design and dynamic control of the HMDV inertial suspension based on the ground-hook positive real network," *Advances in Engineering Software*, vol. 171, Article ID 103171, 2022.

[2] J. Hua, Y. J. Shen, X. F. Yang, Y. Zhang, and Y. L. Liu, "Optimal design of fractional-order electrical network for vehicle mechatronic ISD suspension using the structure-immittance approach," *World Electric Vehicle Journal*, vol. 14, no. 1, p. 12, 2023.

[3] Y. Qin, Z. Wang, K. Yuan, and Y. Zhang, "Comprehensive analysis and optimization of dynamic vibration-absorbing structures for electric vehicles driven by in-wheel motors," *Automotive Innovation*, vol. 2, no. 4, pp. 254–262, 2019.

[4] Y. Qin, Z. Zhao, Z. Wang, and G. Li, "Study of longitudinal–vertical dynamics for in-wheel motor-driven electric vehicles," *Automotive Innovation*, vol. 4, no. 2, pp. 227–237, 2021.

[5] Y. J. Shen, J. Hua, W. Fan, Y. L. Liu, X. F. Yang, and L. Chen, "Optimal design and dynamic performance analysis of a fractional-order electrical network-based vehicle mechatronic ISD suspension," *Mechanical Systems and Signal Processing*, vol. 184, Article ID 109718, 2023.

[6] M. C. Smith, "Synthesis of mechanical networks: the inerter," *IEEE Transactions on Automatic Control*, vol. 47, no. 10, pp. 1648–1662, 2002.

[7] K. Wang, M. Z. Q. Chen, C. Li, and G. Chen, "Supplementary material to: passive controller realization of a biquadratic impedance with double Poles and zeros as a seven-element series-parallel network for effective mechanical control," *IEEE Transactions on Automatic Control*, vol. 63, no. 9, pp. 3010–3015, 2018.

[8] F. J. Li, X. P. Li, D. Y. Shang, and Z. Wang, "Dynamic modeling and damping performance improvement of two stage ISD suspension system," *Proceedings of the Institution of Mechanical Engineers-Part D: Journal of Automobile Engineering*, vol. 236, no. 10-11, pp. 2259–2271, 2022.

[9] M. Mao, L. Wang, Y. J. Chen, Q. S. Lei, and F. Du, "Research progress in inerter and inerter-spring-damper suspension," *Acta Armamentarii*, vol. 37, p. 525, 2016.

[10] R. C. Wang, Q. Ye, Z. Y. Sun, W. Q. Zhou, Y. C. Cao, and L. Chen, "A study of the hydraulically interconnected inerter-spring-damper suspension system," *Mechanics Based Design of Structures and Machines*, vol. 45, no. 4, pp. 415–429, 2017.

[11] X. P. Li, F. J. Li, and D. Y. Shang, "Dynamic characteristics analysis of ISD suspension system under different working conditions," *Mathematics*, vol. 9, p. 1345, 2021.

[12] L. Chen, Y. J. Shen, X. F. Yang, R. C. Wang, X. L. Zhang, and D. H. Shi, "Design and experiment of vehicle suspension based on inerter-spring structure," *Journal of Vibration and Shock*, vol. 22, pp. 83–87, 2014.

[13] X. F. Yang, L. Yan, Y. J. Shen, H. C. Li, and Y. L. Liu, "Dynamic performance analysis and parameters perturbation study of inerter–spring–damper suspension for heavy vehicle," *Journal of Low Frequency Noise, Vibration and Active Control*, vol. 40, pp. 1335–1350, 2020.

[14] M. F. Soong, R. Ramli, A. A. Saifizul, K. Y. Goh, and S. X. Long, "Investigation of inerter-based suspension systems for heavy vehicles," *PLoS One*, vol. 18, no. 1, 2023.

[15] F. Ding, H. Y. Shan, X. Han, C. Jiang, C. Peng, and J. Liu, "Security- based resilient triggered output feedback lane keeping control for HumanMachine cooperative steering intelligent heavy truck under denial-of-service attacks," *IEEE Transactions on Fuzzy Systems*, vol. 31, no. 7, pp. 2264–2276, 2023.

[16] Q. H. Zhang, J. G. Lu, J. Xu, and Y. Q. Chen, "Solution analysis and novel admissibility conditions of SFOSs: the $1<\alpha<2$ case," *IEEE Transactions on Systems, Man, and Cybernetics: Systems*, vol. 52, no. 8, pp. 5056–5067, 2022.

[17] O. Bingul and A. Yildiz, "Fuzzy logic and proportional integral derivative based multi-objective optimization of active suspension system of a 4×4 in-wheel motor driven electrical vehicle," *Journal of Vibration and Control*, vol. 29, no. 5-6, pp. 1366–1386, 2023.

[18] F. Ding, X. Han, C. Jiang, J. Liu, and C. Peng, "Fuzzy dynamic output feedback force security control for hysteretic leaf spring hydro-suspension with servo valve opening predictive management under deception attack," *IEEE Transactions on Fuzzy Systems*, vol. 30, no. 9, pp. 3736–3747, 2022.

[19] J. H. Zhang, J. Liu, and F. Ding, "Collaborative optimization design framework for hierarchical filter barrier control suspension system with projection adaptive tracking hydraulic actuator," *Nonlinear Dynamics*, vol. 108, no. 4, pp. 3417–3434, 2022.

[20] Y. J. Shen, A. Chen, F. Du, X. F. Yang, Y. L. Liu, and L. Chen, "Performance enhancements of semi-active vehicle air ISD suspension," *Proceedings of the Institution of Mechanical Engineers-Part D: Journal of Automobile Engineering*, 2024.

[21] Z. Lu, H. R. Zhang, and S. F. Masri, "Studies on vibration control effects of a semi-active impact damper for seismically excited nonlinear building," *Smart Structures and Systems*, vol. 24, pp. 95–110, 2019.

[22] Z. Lu, M. Y. Zhou, J. W. Zhang, Z. K. Huang, and S. F. Masri, "Experimental and numerical study on the dynamic behavior of a semi-active impact damper," *Smart Structures and Systems*, vol. 31, pp. 455–467, 2023.

[23] D. Karnopp, M. J. Crosby, and R. A. Harwood, "Vibration control using semi-active force generators," *Journal of engineering for industry*, vol. 96, no. 2, pp. 619–626, 1974.

[24] X. J. Zhang, M. Ahmadian, and K. H. Guo, "On the benefits of semi-active suspensions with inerters," *Shock and Vibration*, vol. 19, no. 3, pp. 257–272, 2012.

[25] D. Karnopp and M. J. Crosby, "The active damper a new concept for shock and vibration control," *The Shock and Vibration Bulletin*, vol. 143, pp. 119–133, 1973.

[26] S. M. Savaresi, E. SilanI, and S. Bittanti, "Acceleration-driven-damper (ADD): an optimal control algorithm for comfort-oriented semiactive suspensions," *Journal of Dynamic Systems, Measurement, and Control*, vol. 127, no. 2, pp. 218–229, 2005.

[27] R. Morselli and R. Zanasi, "Control of port Hamiltonian systems by dissipative devices and its application to improve the semi-active suspension behaviour," *Mechatronics*, vol. 18, no. 7, pp. 364–369, 2008.

[28] B. A. Negash, W. You, J. Lee, C. Lee, and K. Lee, "Semi-active control of a nonlinear quarter-car model of hyperloop capsule vehicle with Skyhook and Mixed Skyhook-Acceleration Driven Damper controller," *Advances in Mechanical Engineering*, vol. 13, no. 2, 2021.

[29] Y. Liu and L. Zuo, "Mixed skyhook and power-driven-damper: a new low-jerk semi-active suspension control based on power flow analysis," *Journal of Dynamic Systems, Measurement, and Control*, vol. 138, no. 8, Article ID 081009, 2016.

[30] A. Yildiz, "A comparative study on the optimal non-linear seat and suspension design for an electric vehicle using different population-based optimisation algorithms," *International Journal of Vehicle Design*, vol. 80, no. 2/3/4, pp. 241–256, 2019.

[31] Y. J. Shen, M. Q. Jia, X. F. Yang, Y. L. Liu, and L. Chen, "Vibration suppression using a mechatronic PDD-ISD-combined vehicle suspension system," *International Journal of Mechanical Sciences*, vol. 250, Article ID 108277, 2023.

[32] J. S. Wang, Y. J. Shen, F. Du, M. Li, and X. F. Yang, "Topology optimization design and dynamic performance analysis of inerter-spring-damper suspension based on power-driven-damper control strategy," *World Electric Vehicle Journal*, vol. 15, no. 1, p. 8, 2023.

[33] X. F. Yang, H. Song, Y. J. Shen, and Y. L. Liu, "Study on adverse effect suppression of hub motor driven vehicles with inertial suspensions," *Proceedings of the Institution of Mechanical Engineers-Part D: Journal of Automobile Engineering*, vol. 236, no. 5, pp. 767–779, 2022.

[34] X. Q. Sun, L. Chen, S. H. Wang, C. C. Yuan, and X. L. Zhang, "Nonlinear modeling and parameter optimization of two-stage series-connected ISD suspension," *Transactions of the Chinese Society for Agricultural Machinery*, vol. 45, pp. 7–13, 2014.

[35] X. F. Yang, L. Chen, Y. J. Shen, and R. C. Wang, "Research on vehicle passive ISD suspension with simple three element structure," *Journal of Machine Design*, vol. 30, pp. 42–47, 2013.